The Structure and Dynamics of a Bluff-Body Stabilized Premixed Reacting Flow

Conference Paper · January 2018

DOI: 10.2514/6.2018-1190

7 authors, including:

Tongxun Yi
Spectral Energies LLC
48 PUBLICATIONS **419** CITATIONS
SEE PROFILE

Brent Rankin
Wright-Patterson Air Force Base
64 PUBLICATIONS **368** CITATIONS
SEE PROFILE

Joseph D Miller
67 PUBLICATIONS **997** CITATIONS
SEE PROFILE

AIAA SciTech Forum
8–12 January 2018, Kissimmee, Florida
2018 AIAA Aerospace Sciences Meeting

10.2514/6.2018-1190

The Structure and Dynamics of a Bluff-Body Stabilized Premixed Reacting Flow

Christopher A. Fugger[1] and Tongxun Yi[2]
Spectral Energies, LLC, Dayton, OH, 45431

Joshua P. Sykes[3]
Innovative Scientific Solutions, Inc, Dayton, OH, 45459

Andrew W. Caswell[4], Brent A. Rankin[4], Joseph D. Miller[4], James R. Gord[5]
Air Force Research Laboratory, Wright-Patterson Air Force Base, Dayton, OH, 45433

The structure and dynamics of a confined, premixed propane-air, turbulent bluff-body-stabilized flame are considered. The flow and flame interactions are imaged using simultaneous 10-kHz formaldehyde (CH_2O) planar laser-induced fluorescence (PLIF), OH-PLIF, and particle image velocimetry (PIV). This paper also aims to briefly introduce our bluff-body combustion experiment with a goal of providing spatially-temporally resolved measurement datasets for simulation validation.

Nomenclature

PLIF	=	planar laser-induced fluorescence
PIV	=	particle image velocimetry
D	=	equilateral bluff-body triangle dimension
FWHM	=	full width at half maximum
SNR	=	signal-to-noise ratio
2D	=	two-dimensional

I. Introduction

Propulsion systems employ bluff-body flameholders to stabilize the combustion in high-speed flows. The bluff-body obstruction creates and sustains a hot, radical-rich, lower-velocity recirculation region that ignites the incoming reactants. For a single and ducted bluff-body, the geometric simplicity, the quasi two-dimentional bulk flow, and its relevance to aerospace devices has motivated substantial experimental and computational efforts, notably centered around the Volvo test case.[1–4] Challenges still being addressed regarding the bluff-body reacting flowfield include lean blow off, combustion instabilities, and the predictive accuracy of combustion Large Eddy Simulations.

The bluff-body contains a rich set of physics between the turbulence, hydrodynamics, chemistry, and acoustics. It consists (in part) of shear layer vortex dynamics, the counter-rotating recirculation dynamics behind the bluff-body, and a larger sinuous wake structure (predominantly at low flame density ratios).[5–7] Near lean blow off, transient interactions between flame stabilization, extinction, and hydrodynamics under vitiated inlet conditons (or low density ratios) becomes increasingly nonlinear.[8,9] The flowfield is also highly complex under a thermo-acoustic combustion instability, where the flame excites and sustains the resonant combustor pressure oscillation(s).[1,10] Additionally, flame-wall interactions can be an important process.

[1] Research Engineer, 5100 Springfield St, Suite 301, AIAA Member, Corresponding author.
[2] Research Scientist, 5100 Springfield St, Suite 301, AIAA Member.
[3] Research Engineer, 7610 McEwen Rd., AIAA Member.
[4] Research Engineer, 1790 Loop Rd., AIAA Member.
[5] Principal Research Chemist, 1790 Loop Rd., AIAA Fellow.

One advantage of the single bluff-body configuration is that the nearfield is approximately two-dimensional (2D). Quasi 2D flows are more amenable to planar diagnostics extracting the primary strain components and tracking the flame front motions. Simulataneous measurements of high-speed OH planar laser-induced fluorescence (OH-PLIF) and particle image velocimetry (PIV) have had great success in characterizing 2D and 3D flows.[11–16] More recently, high-speed CH_2O-PLIF emerged as a potentially viable and practical diagnostic. CH_2O-PLIF shows the preheat zone, illustrates the turbulence-flame interactions (e.g., preheat zone broadening), and the overlap of CH_2O-PLIF and OH-PLIF in premixed flames is used to visualize the reaction zone.[17–18]

High-repitition-rate CH_2O-PLIF has only been demonstrated a few times.[19–25] The primary challenge with CH_2O-PLIF is it requires high individual pulse energies, typically higher than that provided by a high-repitition-rate continuous diode-pumped solid-state laser. The present work extends high-repetition-rate CH_2O-PLIF to a larger FOV (> 170 cm^2) with high SNR (47:1 during PIV seed flow), and to its simultaneous use with OH-PLIF/PIV. The CH_2O-PLIF is enabled by a burst-mode laser delivering 10-kHz pulse trains of 355-nm at 350 mJ/pulse.

The purpose of this paper is to update the community on the 10-kHz CH_2O-PLIF, OH-PLIF and PIV measurements completed and ongoing. One goal is providing new insights on bluff-body combustion flows and another is providing high-quality measurement datasets for simulation validation.

II. Experimental Setup

A. Experimental Arrangement

Figure 1 shows the atmospheric-pressure bluff-body-stabilized combustor experimental arrangement and laser diagnostic setup. Preheated, unvitiated air and propane are mixed upstream of the test section. The reactants flow into an optically-accessible rectangular duct with a cross-section of 152.4 mm (H) in the spanwise direction and 127 mm in the transverse direction. The bluff body is a solid 38.1 mm (D) equilateral triangle. The test section exit is open to the atmosphere. Nominal fuel and air equivalence ratios range between 0.5–1.2, and nominal non-vitiated electrically-preheated are temperatures range between 300–700 K.

High-frequency pressure transducers (HFPT) mounted in a semi-infinite tube configuration are located along the streamwise and transverse directions. The HFPT's are recorded at 100 kHz. The acoustics are temporally well-resolved; the dominant longitudinal resonant chamber acoustics are below 500 Hz, and the predicted transverse acoustic modes are below 5 kHz. The camera triggers and exposures are simultaneously recorded on the high-frequency data system, and during data post-processing the imaging and pressure data are temporally aligned.

Two operating conditions are presented in this paper. Both conditons are for an air massflow of 0.35 kg/s and a premixed air-fuel mixture temperature of 310 K. The Reynolds number (based on D) and Mach number at the bluff body trailing edge are 54000 and 0.06, respectively. Based on calculated turbulent scaling parameters using the PIV measurements to calculate the integral length and time scales, both cases are in the broadened preheat, thin reaction zone regime.

B. Laser Diagnsostic Measurements

The 10 kHz CH_2O-PLIF is performed using the high pulse energies at 355-nm from a quasi-continuous burst-mode (QCBM) laser (QuasiModo, Spectral Energies, LLC).[26] The frequency-tripled QCBM laser produces a 10-kHz pulse train of 355-nm 10-ns pulses, in 10.5-ms bursts, at every 12 s. Individual pulses have an energy of approximately 350 mJ. An expanding laser sheet is formed using a combination of negative and positive cylindrical lenses. The CH_2O fluorescence is bandpass filtered over 390–520 nm, and images are recorded with a high-speed intensifier coupled to a high-speed camera. A 100-ns intensifier gate captures the CH_2O fluorescence. At 10 kHz, the recording camera array size is 1024 × 1024 pixels, corresponding to 0.16 mm/pixel.

For OH-PLIF, a 10-kHz Nd:YAG laser (Edgewave) pumps a tunable dye laser (Sirah Credo). The output (0.30 mJ/pulse) is tuned to the $Q_1(9)$ transition of OH. An expanding laser sheet is formed using a combination of negative and positive cylindrical lenses. The OH fluorescence is bandpass filtered using a 320/40 filter (Semrock), and images are recorded with a high-speed intensifier coupled to a high-speed camera. A 100-ns intensifier gate captures the OH fluorescence. At 10 kHz, the recorded camera array size is 1024 × 632 pixels, corresponding to 0.19 mm/pixel.

For PIV, an Nd:YAG laser (Edgewave) operating at 10 kHz is used for the 532-nm, double-pulse PIV. The seed is a 0.3 μm Alumina. An expanding laser sheet is formed using a combination of negative and positive cylindrical lenses. The images are acquired using a high-speed camera operating at 20 kHz with a 9-nm FWHM band-pass optical filter. Vector processing is performed using LaVision Davis 8.3.1 software. The light-scattered images are preprocessed with a 16 × 16 pixels sliding background subtraction and 6 × 6 pixels sliding particle intensity normalization. Vector fields are computed using the multipass adaptive-windowing Davis algorithms with a 24 × 24 interrogation window and 50 % overlap. The spatial resolution of the raw light-scattered PIV images is 0.21 mm/pixel, corresponding to a 2.5-mm vector spacing.

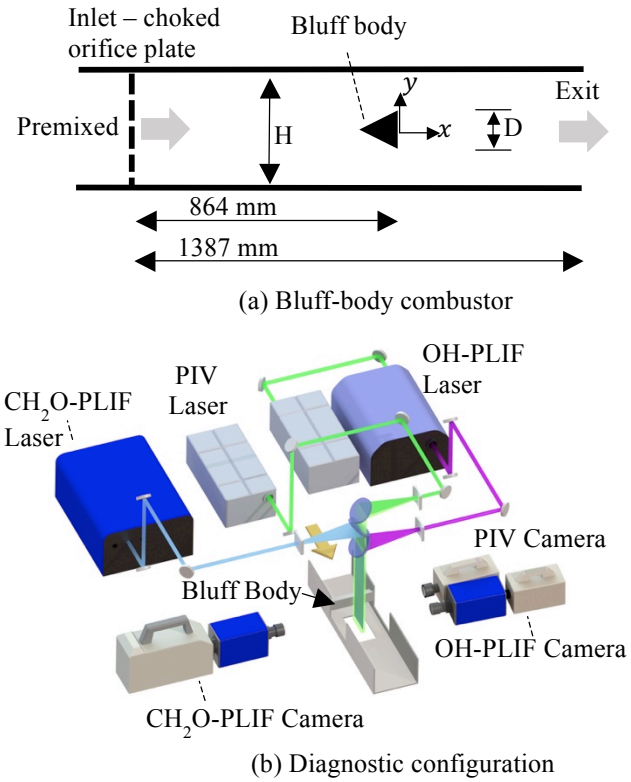

Figure 1. Schematics of the AFRL bluff-body stabilized experimental arrangement. (a) Combustor configuration. (b) laser diagnostic configuration.

The three laser sheets are overlapped spatially with dichroic mirrors, and the laser sheets are centered at the combustor centerline. The 355-nm pulse is centered in the 532-nm pulse pair, and the 283-nm pulse is delayed 150 ns relative to the 355-nm pulse to reduce 355-nm seed scatter, 355-nm induced seed fluorescence, and 355-nm induced quartz window fluorescence background signals.

C. Image processing and Overlap CH_2O/OH

The preheat zone is obtained directly from the CH_2O-PLIF images, and the reaction zone is derived from the pixel-by-pixel product of the CH_2O-PLIF and OH-PLIF images. Calibrations of the PLIF signals for quenching were not done. A qualitative relationship between the reaction zone and the overlap CH_2O-PLIF/OH-PLIF images is assumed.

The CH_2O-PLIF and OH-PLIF raw images are processed to correct for: (i) noise and background chemiluminescence using a time-averaged background image, (ii) spatial nonuniformity of the intensifier using a uniformly illuminated light source, and (iii) laser-sheet nonuniformity using acetone-seeded cold flow images. At this point, the SNR of the CH_2O-PLIF images is 47:1 during PIV seed flow, where SNR is defined by dividing the CH_2O ensemble average by the signal's mean value in regions not containing CH_2O. To extract the edges and the gradients, an iterative connectivity filter is applied along with a thresholding based on the local image statistics. The images are processed during the first iteration with a low-pass filter (2D Wiener), and finished with a gradient-based edge detection scheme.

Laminar flame profiles were calculated using Cantera with the USC II mechanism for propane.[27] Each flame is freely-propagating, premixed, and adiabatic. Figure 2 shows the flame profiles for a propane-air mixture at an equivalence ratio of 0.65 and preheat of 310 K, where the variables are normalized to their peak values. Thickness is defined by the full width at half maximum (FWHM) of the profile. The CH_2O thickness for an equivalence ratio of 0.65 and 0.90 is 0.35 and 0.25 mm, respectively. The heat release and overlap CH_2O/OH are spatially overlapped. For the 0.65 equivalence ratio, the overlap CH_2O/OH thickness is 0.15 mm.

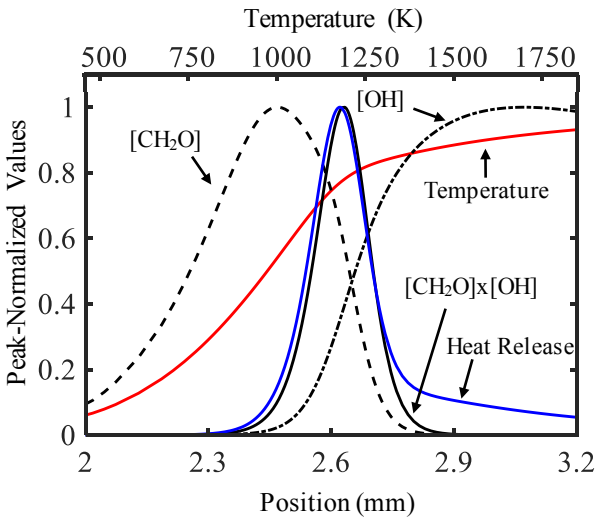

Figure 2. Spatial profiles of CH_2O, OH, the overlap of CH_2O with OH, temperature, and heat release at a propane-air equivalence ratio of 0.65.

III. Results and Discussion

A. Steady Combustion

Figure 3 shows a simultaneous image of velocity (vector arrows), OH-PLIF (red), CH_2O-PLIF (green), and the overlap CH_2O-PLIF/OH-PLIF (yellow) extracted from a 10-kHz measurement sequence. The wake flow behind the bluff body is marked by both the negative velocity and the homogeneous OH-PLIF. The CH_2O-PLIF resides on the reactants side of the flame. The preheat zone (CH_2O) thickness displays a range of thicknesses, up to 10 times the calculated laminar CH_2O thickness. The overlap CH_2O-PLIF/OH-PLIF is relatively thin and nearly continuous everywhere. This agrees with the assessment that the turbulent combustion is in the broadened-preheat, thin reaction zone regime. Certain regions show a thickened overlap CH_2O/OH, but this is likely experimental uncertainty. For the large field-of-view images, the spatial resolution is on the order of the reaction zone thickness. Additionally, the overlap of the multiple cameras to one another contributes to additional uncertainty. Upcoming plans include higher-resolution imaging to accurately resolve the thin reaction zone.

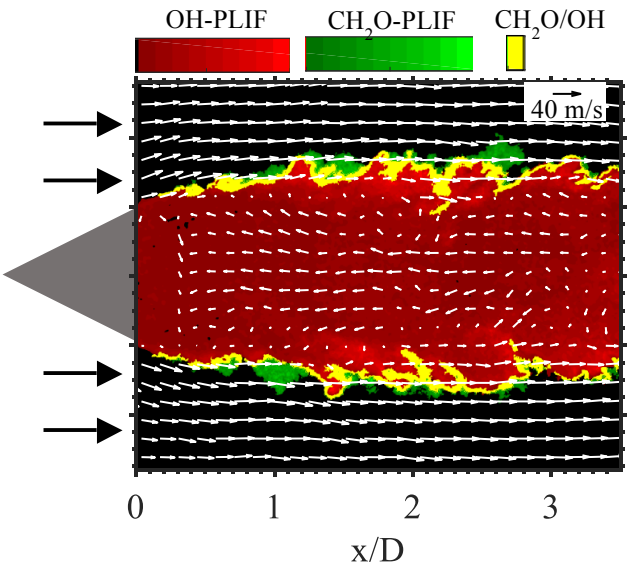

Figure 3. Simultaneous image of the CH_2O-PLIF (green), OH-PLIF (red), overlap of CH_2O-PLIF/OH-PLIF (yellow), and velocity (white vectors). Every other vector is shown for image clarity.

Figure 4 shows three consecutive images of simultaneous vorticity (background contour), CH_2O-PLIF (black contour), and the overlap CH_2O-PLIF/OH-PLIF (magenta curve). The image at 0.2 ms corresponds to the Figure 3 image. The highest levels of vorticity are concentrated to narrow regions in the upper and lower shear layers. The CH_2O is located closer to the center of the highest vorticity near the bluff body, where substantial CH_2O-vortex interactions appear to cause CH_2O accumulation. The overlap OH/CH_2O is nearly uniform across the flowfield. Significant preheat broadening is also observed in a few locations, e.g., (x/D,y/D) = (2.5,0.75). In general for this

operating condition, the measured CH_2O thickness is statistically thicker closer to the bluff body, with a thickness distribution of up to 10 times the calculated laminar CH_2O thickness.

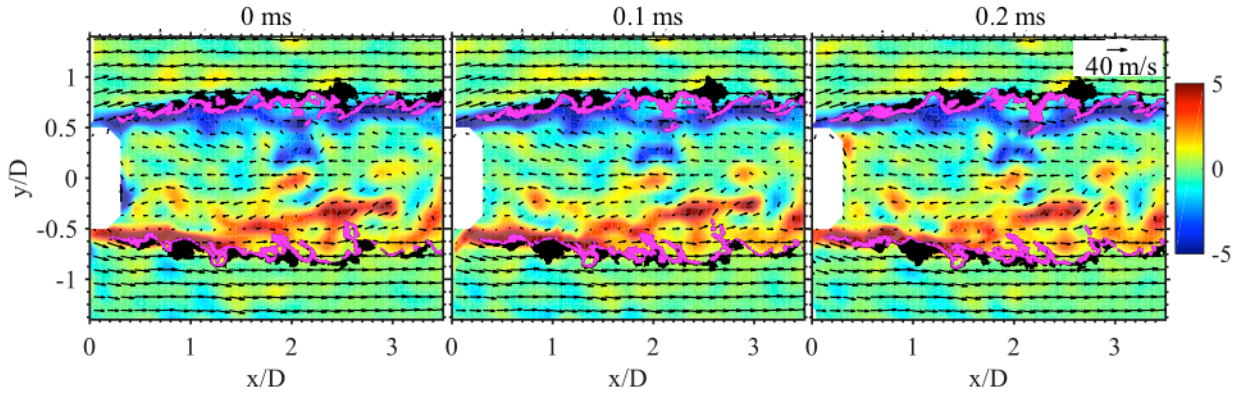

Figure 4. Consecutive images of simultaneous vorticity (background contour, 1000s^{-1}), CH_2O-PLIF (black overlay), and the overlap CH_2O-PLIF/OH-PLIF (magenta curve). Every other vector is shown for image clarity

B. Thermoacoustic Instability

A combustion instability is self-excited at higher equivalence ratios. Figure 5(a) shows a spectrum of the high-frequency pressure transducer near the choked orifice plate. The dominant acoustic oscillation is at 83 Hz, which is the 1L longitudinal acoustic mode between the orifice plate and chamber exit. Minor harmonic frequencies are also present, though with a much weaker amplitude, which is expected for a strongly driven primary instability.

Figure 5(b) shows the pressure bandpass-filtered at 83 Hz over a segment of the 83 Hz period. Three points in time are highlighted (solid circles) in Fig. 5(b) and interrogated further in Fig. 6. Figure 6 shows images of simultaneous CH_2O-PLIF, OH-PLIF, overlap CH_2O-PLIF/OH-PLIF, velocity vectors, and vorticity for the three Fig. 5(b) points. The longituindal instability produces a symmetric velocity oscillation at the bluff body. At 1.4 ms, the flowfield pressure oscillation p' is relieving itself and the flow is accelerating. The vorticity is intense and localized close to the bluff body. The flame is advected downstream, and the flow begins to neck in towards the centerline behind the bluff-body (x/D = 1) . There are distributed regions of CH_2O and OH near the upper wall (y/D > 0), suggesting flame-wall interactions. Nearly the entire region beyond x/D = 1.5 is combustion products. The instability drives the flame back toward the bluff body trailing edge once every cycle.

At 4.1 ms, the flowfield is close to its maximum cycle velocity and the wake filled with combustion products extends to x/D = 3.5. Following the necking of the flowfield shortly after 1.4 ms, the reactants entrained into the wake burn in distributed regions. A vortex structure near (x/D, y/D) = (1.8,0) appears to contribute to mixing the burning reactants in the wake.

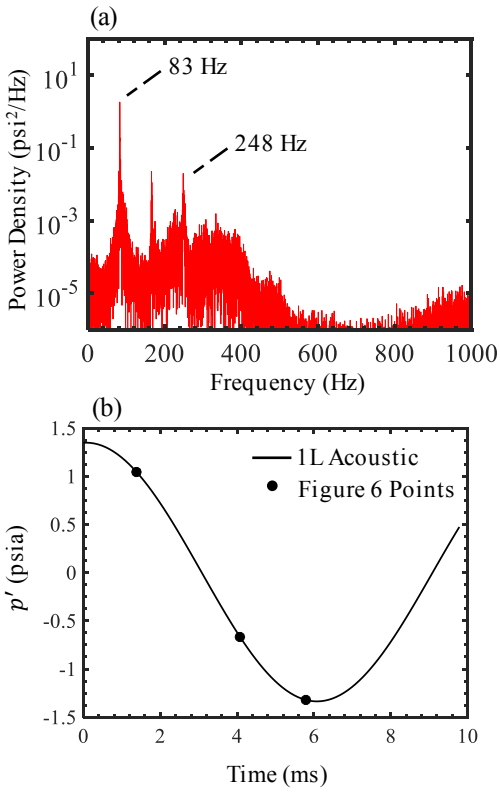

Figure 5. (a) Power spectral density of the high-frequency pressure transducer at the orifice plate. (b) 83 Hz bandpass-filtered pressure over the period corresponding to the images in Fig. 6.

At 5.8 ms, the pressure is near its cycle minimum, the velocity is decelerating, and the vorticity magnitude is reduced. As the flame is moving upstream due to a decreasing approach flow velocity, the wake (filled with combustion products) size is growing. The CH_2O is relatively thin everywhere, as is the overlap CH_2O/OH, which contrasts the thicker CH_2O or overlap CH_2O/OH at 1.4 ms or 4.1 ms. Soon after 5.8 ms, the flame is driven back toward the bluff body trailing edge.

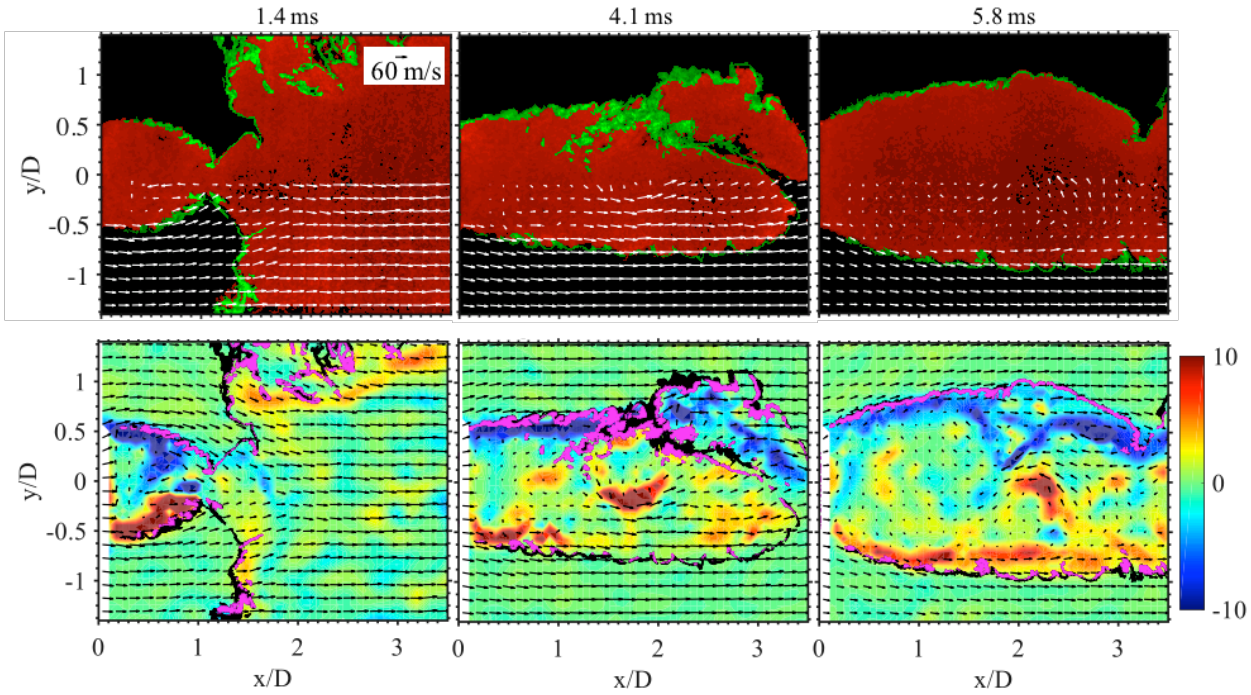

Figure 6. Top row: Simultaneous CH_2O-PLIF (green), OH-PLIF (red), and velocity (white vectors). Every other vector for y/D < 0 is shown for image clarity (includes bottom row). Bottom row: Simultaneous vorticity (background contour, 1000s^{-1}), CH_2O-PLIF (black overlay), and the overlap CH_2O-PLIF/OH-PLIF (magenta curve). The time of the three instances corresponds to Fig. 5(b).

C. Concurrent LES

Computational efforts are being performed in parallel with the experimental work described above. Large eddy simulations (LES) of the bluff body case use VIDA, an incompressible, variable density solver. Combustion effects are modeled with a flamelet progress variable (FPV) approach and dynamic flame thickening (DTF) is used to resolve the flamefront. The nominal mesh size is a 1mm cube and the overall cell count is ~12 million. Figure 7 displays various close-up views of instantaneous results of such a simulation.

Even with meshes clustered in the trailing edge shear layer, it is very difficult to replicate the transient behavior immediately downstream of the bluff body in 3-dimensional LES. The main difficulty lies in capturing the thin flamefront, which here is numerically diffused over several 1mm cells. Capturing the transient wrinkling of the flame in this trailing edge region would necessitate either a much finer mesh (likely 0.25mm nominal at most) or some alternative combustion closure model; high-fidelity modeling of this semi-practical problem may therefore incur computational cost far above that of an "engineering LES" approach.

Other initial comparisons between the LES and experiment indicate that the LES has difficulty capturing the strength of the recirculation zone behind the bluff body. The resulting "wake" structure has also been observed by LES of the Volvo case.[28] Nevertheless the LES here does indeed appear to replicate the experiment's vorticity strength in the shear layer.

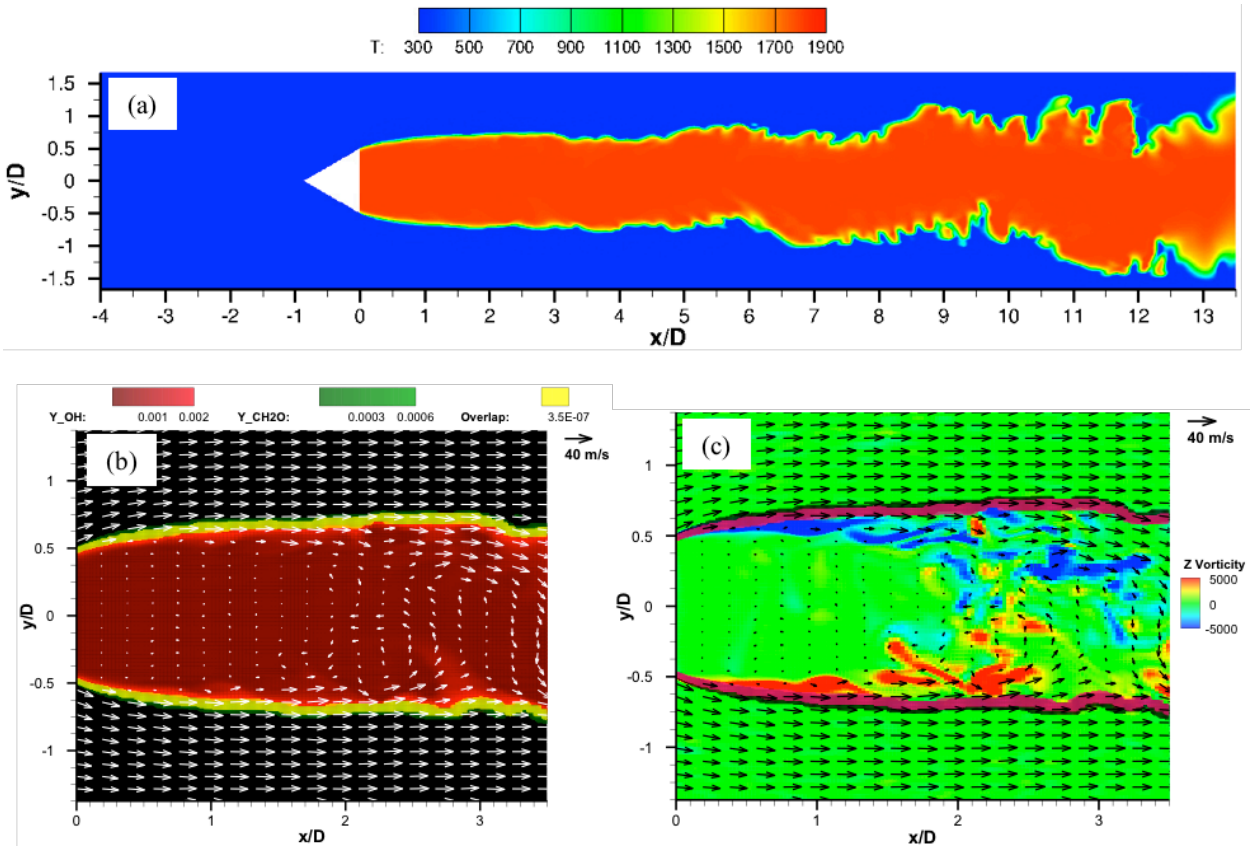

Figure 7. Instantaneous LES results for the 0.35 kg/s air massflow, 0.65 equivalence ratio case. (a) depicts a cross-section temperature contour of the entire numerical domain. (b) depicts contours of OH, CH_2O, and the overlap thereof comparable to Fig. 3. (c) depicts contours of vorticity (1/s), CH_2O (magenta), and the OH/CH_2O (black) overlap comparable to Fig. 4. Although the computational mesh is clustered in the shear layer, the figures downsample the location of the velocity vectors for visibility and comparison to the PIV.

IV. Summary and Conclusion

Measurements on a confined, premixed, propane-air bluff-body-stabilized flame are presented. Simultaneous 10-kHz CH_2O-PLIF, OH-PLIF, and PIV are used to image the preheat zone, the reaction zone, and the velocity field during a statistically-steady and combustion instability case.

Acknowledgments

This work was funded by the Air Force Research Laboratory. This work has been cleared for public release by AFRL (No. 88ABW-2017-5915). The authors would like to thank Sukesh Roy for research guidance and discussions, Ethan Legge for assisting with the diagnostics setup and execution, Brendan Paxton and Steve Britton for assisting with the combustor operation, and Jeffrey Monfort for assistance with the high-frequency pressure measurements.

References

[1]Sjunnesson, A., Olovson, S., Sjoblom, B., "Validation Rig – A Tool for Flame Studies," International Society for Air-Breathing Engines Conference, ISABE-91-7038, Nottingham, United Kingdom, 1991.
[2]Sjunnesson, A., Henrikson, P., Lofstrom, C., "CARS Measurements and Visualization of Reacting Flows in a Bluff Body Stabilized Flame," AIAA Joint Propulsion Conference, Nashville, TN, 1992. AIAA 92-3650.
[3]Fureby, C., Moller, S.I., "Large Eddy Simulation of Reacting Flows Applied to Bluff-Body Stabilized Flames," AIAA Journal,

Vol. 33, No. 12, 1995, pp 2339–2347.
[4]Comer, A., Ihme, M., Li, C., Menon, S., Oefeline, J., Rankin, B., Sankaran, V., Sankaran, V., (Eds.). "First Model Validation for Propulsion Workshop," Accessed online November 2017, https://community.apan.org/wg/afrlcg/mvpws/p/proceedings, 2017.
[5]Prasad, A., Williamson, C.H.K., "The Instability of the Shear Layer Separating from the Bluff Body," *Journal of Fluid Mechanics*, Vol. 333, 1997.
[6]Erickson, RR., Soteriou, M.C. "The Influence of Reactant Temperature on the Dynamics of Bluff Body Stabilized Premixed Flames," *Combustion and Flame*, Vol. 158, 2011.
[7]Emerson, B., O'Connor, J., Juniper, M., Lieuwen, T., "Density Ratio Effects on Reacting Bluff-Body Flow Field Characteristics." *Journal of Fluid Mechanic,* Vol. 706, 2012.
[8]Shanbhogue, S.J., Husain, S., Lieuwen, T., "Lean Blowoff of Bluff Body Stabilized Flames: Scaling and Dynamics," *Progress in Energy and Combustion Science*, Vol. 35, 2009, pp 98 –120.
[9]Tuttle, S.G., Chaudhuri, S., Kostka, S., Kopp-Vaughan, K.M., Jensen, T.R., Cetegen, B.M., Renfro, M.W., "Time-Resolved Blowoff Transition Measurements for Two-Dimensional Bluff-Body-Stabilized Flames in Vitiated Flows," *Combustion and Flame*, Vol. 159, 2012, pp 291–302.
[10]Kostka, S., Lynch, A.C., Huelskamp, B.C., Kiel, B.V., Gord, J.R., Roy, S., "Characterization of Flame-Shedding Behavior Behind a Bluff-Body Using Proper Orthogonal Decomposition," *Combustion and Flame*, Vol. 159, 2012, pp 2872–2882.
[11]Meier, W., Boxx, I., Stohr, M., C.D. Carter, "Laser-based investigations in gas turbine models combustors," Experiments in Fluids, 2010, Vol. 49, pp 865-882.
[12]Steinberg, A.N., Boxx, I., Stohr, M.m Carter, C.D., Meijer, W., "Flow-flame interactions causing acoustically coupled heat release fluctuations in a thermos-acoustically unstable gas turbine model combustor," Combustion and Flame, Vol. 157, 2010, pp 2250-2266.
[13]Boxx, I., Arndt, C.M., Carter, C., Meier, W., "High-speed laser diagnostics for the study of flame dynamics in a lean premixed gas turbine model combustor," Experiments in Fluids, 2012, Vol 52, pp 555-567
[14]Slabaugh, C.D., Pratt, A.C., Lucht, R.P., "Simultaneous 5 kHz OH-PLIF/PIV for the study of turbulent combustion at engine conditions," Applied Physics B, (2015). (118). pp 109-130.
[15]Caswell, A.W., Rankin, B.A., Huelskamp, B.C., Lynch, A.C., Belovich, V., Gord, J.R., "Spatiotemporal Characterization of Bluff-Body Stabilized Turbulent Premixed Flames Using Simultaneous High-Repitition-Rate OH PLIF and PIV Measurements," 53rd AIAA Aerospace Sciences Meeting, Kissimmee Florida, AIAA 2015-0424.
[16]Chterev, I., Rock, N., Ek, H., Emerson, B., Seitzman, J., Jiang, N., Roy, S., Lee, T., Gord, J., Lieuwen, T., "Simultaneous imaging of fuel, OH, and three component velocity fields in high pressure, liquid fueled, swirl stabilized flames at 5 kHz," Combustion and Flame, Vol. 186. 2017. Pp 150-165.
[17]Paul, P.H., Najm, H.N., "Planar Laser-Induced Fluorescence Imaging of Flame Heat Release Rate," Twenty-Seventh Symposium (International) on Combustion, 1998, pp 43–50.
[18]Skiba, A.W., Wabel, W.M., Temme, J.E., Driscoll, J.F., "Experimental Assessment of Premixed Flames Subjected to Extreme Turbulence," AIAA SciTech Forum, San Diego, CA, 2016.
[19]Gabet, K.N., Patton, R.A., Jiang, N., Lempert, W.R., Sutton J.R., "High-speed CH_2O PLIF imaging in turbulent flames using a pulse-burst laser system," Applied Physics B, 2012, Vol. 106, pp 569-575.
[20]Michael, J.B., Venkateswaran, P., Miller, J.D., Slipchenko, M.N., Gord, J.R., Roy, S., Meyer, T.R., "100 kHz Thousand-Frame Burst-Mode Planar Imaging in Turbulent Flames," *Optics Letters* 39 (4) (2014) 739–742.
[21]Halls, B.R., Jiang, N., Meyer, T.R., Roy, S., Slipchenko, M.N., Gord, J.R., "4D Spatiotemporal Evolution of Combustion Intermediates in Turbulent Flames Using Burst-Mode Volumetric Laser-Induced Fluorescence," *Optics Letters* 42 (14) (2014) 2830–2833.
[22]Allison, P.M., Chen, Y., Ihme, M., Driscoll, J.F., "Coupling of Flame Geometry and Combustion Instabilites Based on Kilohertz Formaldehyde PLIF Measurements," *Proceedings of the Combustion Institute*, Vol. 35, 2015. pp 3255–3262.
[23]Osborne, J.R., Ramji, S.A., Carter, C.D., Peltier, S., Hammack, S., Lee, T., Steinberg, A.M., "Simultaneous 10 kHz TPIV, OH PLIF, and CH_2O PLIF Measurements of Turbulent Flame Structure and Dynamics," *Experiments in Fluids*, Vol. 57, Issue 5, 2016, pp 57–65.
[24]Miller, J.D., Peltier, S.J., Slipchenko, M.N., Mance, J.G., Ombrello, T.M., Gord, J.R., Carter, C.D., "Investigation of transient ignition processes in a model scramjet pilot cavity using simultaneous 100 kHz formaldehyde planar laser-induced fluorescence and CH* chemiluminescence imaging," *Proc. Combust. Inst.* 36 (2017) 2865–2872.
[25]Z. Li, J. Rosell, M. Alden, M. Richter, "Simultaneous Burst Imaging of Dual Species Using Planar Laser-Induced Fluorescence at 50 kHz in Turbulent Premixed Flames," *Appl. Spectroscopy* 71 (6) (2017) 1363–1367.
[26]Slipchenko, M.N., Miller, J.D., Roy, S., Gord, J.R., Danczyk, S.A., Meyer, T.R., "Quasi-Continuous Burst-Mode Laser for High-Speed Planar Imaging," Optics Letters, Vol. 37, No. 8, 2012. pp 1346–1348.
[27]Wang, H., You, X., Joshi, A.V., Davis, S.G., Laskin, A., Egolfopoulos, Law, C.K., USC Mech Version II. High-Temperature Combustion Reaction Model of H2/CO/C1-C4 Compounds. http://ignis.usc.edu/USC_Mech_II.htm, May 2007.
[28]Sankaran, V., Gallagher, T.P., "Grid Convergence in LES of Bluff Body Stabilized Flames," 55th AIAA Aerospace Sciences Meeting, Grapevine Texas, AIAA 2017-1791.